Journal of CO2 Utilization 56 (2022) 101842

Contents lists available at ScienceDirect

Journal of CO2 Utilization

journal homepage: www.elsevier.com/locate/jcou

A potentially non-contact monitor method for CO_2 at the pseudo-critical region using infrared spectrometer

Kaixiang Xing, Yuxuan Ji, Zheng Wang, Mingxuan Wang, Yafei Liu, Haoran Xu, Gang Xiao *

State Key Laboratory of Clean Energy Utilization, Zhejiang University, 38 Zheda Road, Hangzhou, 310027, China

ARTICLE INFO

Keywords:
Supercritical carbon dioxide
Characteristic spectrum
Critical opalescence
Near infrared spectroscopy
Monitor method

ABSTRACT

Supercritical carbon dioxide (sCO_2) Brayton cycle is a promising choice for thermal power generation with the advantages of high efficiency, compactness and low cost. There is a very sensitive part for monitor and control in the cycle, i.e. CO_2 at the critical region, which affects the efficiency of compressor greatly and maybe brings safety problems due to the rapid and great changes in the properties of CO_2 near the critical point. A non-contact measurement method is proposed to monitor the transient state of CO_2 at various operating conditions using an infrared spectrometer. Experimental investigations were carried out to verify the adaptability of the method at dynamic processes in transcritical CO_2 loop tests. We found the density change of CO_2 fluid can directly impact the absorption spectrum near the wavelength of 3400 nm, which could serve as an efficient signal of CO_2 state changes. In a steady state, a dramatic reduction of the density (− 70 %) and the absorption ratio (− 60 %) were observed between 30 and 34 °C. In the dynamic processes, density-related scattering phenomena were observed near the pseudo-critical points, which strengthened the non-transmissive ratio (up to 0.95) of CO_2 and gave a quick signal (<1 s) whenever abnormal condition occurred. Density stratification was further observed in the heating process at 32.5 °C and 7.5 MPa, which was close to the critical point. Moreover, the gasification time was more than five times longer than the liquefaction time, which caused a stronger scattering phenomenon in depressurization processes. This work is expected to serve as the foundation work of the potentially non-contact monitor in the sCO_2 Brayton cycle or other applications.

1. Introduction

Supercritical carbon dioxide (sCO_2) functions widely as a media for reaction [1], extraction [2,3], separation, mass transport [4,5] and heat transfer [6–8]. Its characteristic is extremely important in the sCO_2 Brayton cycle, which is one of the most promising power generation systems with the advantages of compactness, low cost and high efficiency [9]. To reach a high efficiency, an operating state close to the critical point is needed at the compressor inlet of the sCO_2 Brayton cycle [10]. But it is impractical in operation due to the appearance of density change in dynamic processes, which may cause a severe damage in abnormal conditions. The CO_2 flow near the critical point is the compressible turbulent field, whose thermodynamic parameters are fluctuating greatly over space and time. Traditional measuring method suffers from problems such as flow field following, flow-field disturbing [11] and significant measuring deviation. Besides, the density of CO_2 is sensitive with the temperature and pressure, as shown in Fig. 1(a) [12]. The peak value of heat capacity appears at the pseudo-critical points as shown in Fig. 1(b) [12]. However, the instruments can hardly get accurate data timely from the system (especially the temperature data) and hardly present the dynamic characteristics of system during starting up, shutting down or other changing conditions. Therefore, a new-type method is needed to monitor the density changes of sCO_2 near the pseudo-critical points [13].

Spectroscopy is the study of the interaction between matter and electromagnetic radiation as a function of the wavelength or frequency of the radiation, which is a fundamental exploratory tool in the fields of physics, chemistry, and astronomy. Since firstly studied by Einstein [14], the critical characteristics of various gases, such as H_2O, CO_2 and N_2, are widely studied by researchers with the Raman spectroscopy [15–19]. In recent two decades, several studies have focused on the characteristics of CO_2 near the critical point. Nakayama et al. studied the density fluctuation of CO_2 in the supercritical region [20] and proposed gas- and liquid-like regions based on the ridge of density fluctuation to explain the dynamic behavior continuity of CO_2 cross the critical point. Arakcheev at al. adopted the coherent anti Stokes Raman scattering to investigate the vibrational spectrum of the Q bands of 1388/1285 cm^{-1}

* Corresponding author.
E-mail address: xiaogangtianmen@zju.edu.cn (G. Xiao).

https://doi.org/10.1016/j.jcou.2021.101842
Received 13 August 2021; Received in revised form 13 October 2021; Accepted 2 November 2021
Available online 3 December 2021

Nomenclature

Abbreviations

Eq	Equation
sCO_2	Supercritical carbon dioxide

Roman alphabet

C	Fluid concentration (mol L^{-1})
C_{60}	Footballene
I	Transmission intensity (a.u.)
K	Molar absorption coefficient (L mol^{-1} m^{-1})
L	Absorption thickness (m)
x	Measurement deviation

Greek symbols

ρ_c	Critical density (kg m^{-3})
ε	Non-transmissive ratio
σ	Absorption ratio
δ	Scattering ratio

Subscripts and superscripts

B	With the light source
i	The value for group i
s	With a vacuum container
T	Without the light source

characteristic absorption bands in the infrared spectrum is adopted.

As the characteristic absorption bands are primarily determined by the atomic and molecular composition, infrared spectrum is widely used as monitor or measurement method in relative fields. Infrared spectrum monitor has the advantages of flexible, accurate and stable, which was designed to measure the ambient temperature in the room [26]. Román-Ospino et al. [27] proposed to use near infrared spectroscopic calibration models as real time monitor of powder density in the flow, which can provide accurate data timely. Besides, CO_2 has characteristic infrared absorption bands in the infrared wavelength of 1000–5000 nm. Therefore, we selected the infrared spectrum as the monitor method of CO_2, whose absorption ratios are higher than 0.3 at the supercritical state, offering stronger signal during the dynamic process near the critical point.

To develop a compact system, a sCO_2 loop with an infrared spectrum device is employed in this study. The effects of various working conditions, including the operating temperature and pressure, the heating process, the boost process and the depressurization process are fully investigated. The absorption ratio and the scattering ratio near the critical point are compared with the experimental results to verify the sensitivity and accuracy of this non-contact method. This study is expected to build a solid foundation for the non-contact measurement of sCO_2 in various applications.

2. Methods and equipment

2.1. Experimental details

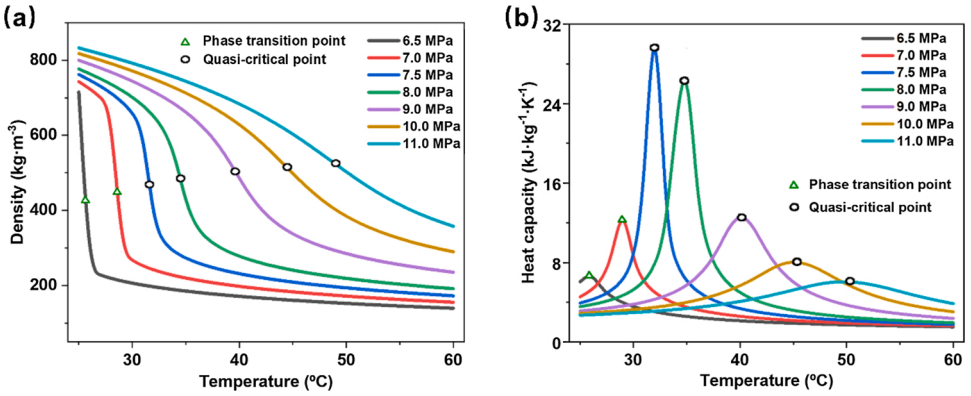

Fig. 1. The physical properties of CO_2 with pressure ranging from 6.5 MPa to 11.0 MPa, and temperature ranging from 25 °C and 60 °C: (a) density variation, (b) heat capacity variation.

under the compression of liquid CO_2 [21], where they found the progressive narrowing of the spectral contribution was attributed to the collapsed rotational structure. They also studied the broadening peculiarities of vibrational bands near the critical temperature [22], where they found the width of *Q* bands did not increase above the critical density ρ_c, while the width of low frequency *Q* band continues to decrease until the density reached 1.7 ρ_c. Chaikina used the Raman spectrum to study the broadening of vibration *Q* bands caused by the fluctuation of critical density, and found that the variance was less than 0.1 and the duration was within 10 ns [23]. Chaikina also built a molecular model for the critical opalescence of CO_2 to explicitly reckon the contribution of molecular thermal motion to the Rayleigh light scattering in critical medium [24]. Chaikina and Umanskii further studied peculiarities of the small-angle scattering of laser radiation by critical CO_2, and got reliable information at a correlation length of $\sim 10^{-5}$ m and a relative density variance of $\sim 2{\cdot}10^{-4}$ for the large-scale critical fluctuation of CO_2 [25]. However, the Raman spectrum suffers from severe interferences in industrial-level applications due to its weak signal. To exaggerate the absorption signal of CO_2 with high stability, its

As shown in Fig. 2, the infrared absorption spectrum testing system of CO_2 mainly consists of a CO_2 pressure control loop (including a gas source, a condenser, a three-plunger pump, a straight heater and a back-pressure valve) and an infrared absorption spectrum measurement device of CO_2. The loop can provide desired pressures between 6.0 and 15.0 MPa, where the three-plunger pump and the back-pressure valve are used to control the CO_2 flow rate and the working pressure of high-pressure sections, respectively. The fluid temperature in the loop is controlled by the heater. The absorption spectrum measurement device consists of a spectrometer, a light source and a CO_2 container, which can obtain real-time information at changing conditions. The PbSe Array Spectrometer (Special Products) supports a spectral range of 1500–5000 nm with a resolution of 20 −150 nm. The SLS203 L (Thorlabs) light source supports a spectral range of 500–9000 nm with a heating source temperature of 1273 °C, of which the power stability is larger than 99.95 %. The stainless CO_2 container can work at 12.0 MPa between 0 and 500 °C. It is equipped with an Omega thermocouple (± 0.5 °C in accuracy), a pressure sensor (± 0.1 % in accuracy) and two high pure sapphire glass windows (25 mm in diameter, 20 mm in thickness) with the spectral

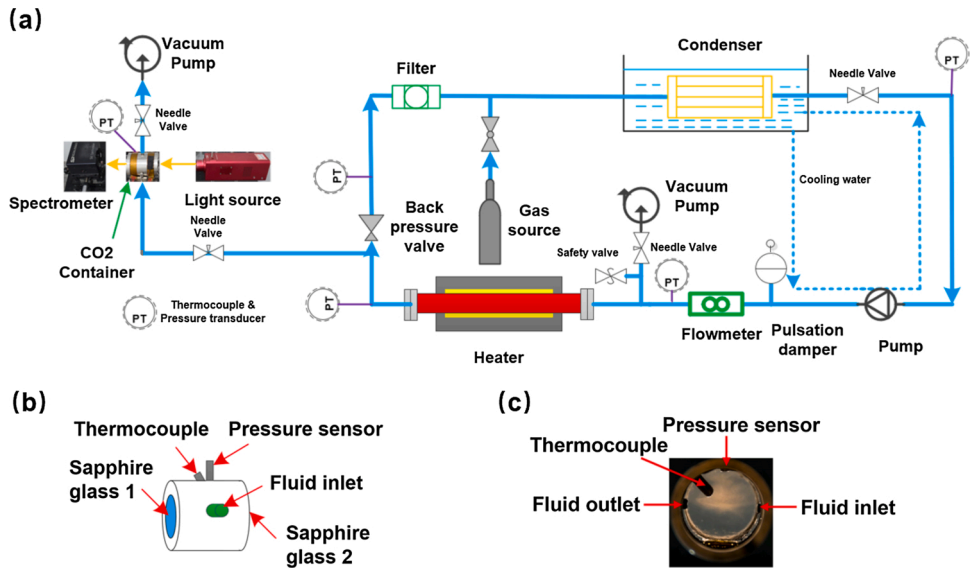

Fig. 2. Infrared absorption spectrum testing system of CO_2: (a) schematic layout, (b) geometry of the CO_2 container, (c) sectional view of the CO_2 container.

Table 1
Various testing conditions for the spectrum absorption testing experiments.

Experiment types	Temperature (°C)	Working pressure (MPa)				
Steady state experiments	25	7	7.5	8	9	10
	30	7	7.5	8	9	10
	35	7	7.5	8	9	10
	45	7	7.5	8	9	10
	55	7	7.5	8	9	10
Heating experiments	23→35	7				
	23→40	7.5				
	24→46	8				
	26→46	9				
	28→50	10				
	36→58	11				
Boost experiments	25	6.5→7	7→7.5	…	10→10.5	10.5→11
	30	6.5→7	7→7.5	…	10→10.5	10.5→11
	35	6.5→7	7→7.5	…	10→10.5	10.5→11
	45	6.5→7	7→7.5	…	10→10.5	10.5→11
Depressurization experiments	25	7→6.5	7.5→7	…	10.5→10	11→10.5
	30	7→6.5	7.5→7	…	10.5→10	11→10.5
	35	7→6.5	7.5→7	…	10.5→10	11→10.5
	45	7→6.5	7.5→7	…	10.5→10	11→10.5

transmittance exceeding 80 % of the test band. The information data can be detected by the thermocouples, pressure sensors and the spectrometer.

Before operation, the needle valve between the CO_2 loop and the CO_2 container (valve1) was closed, while the needle valve between the CO_2 container and the vacuum pump (valve2) was opened, so that the air in the container could be extracted and the light intensity could be measured at a vacuum state. This control group can reduce the influence of the environment and sapphire glass on the test results. Then valve1 and valve2 were switched to open and close states, respectively, and the working pressure and the temperature of CO_2 fluid were adjusted by the back-pressure valve and the film heater, respectively. The detailed testing conditions can be found in Table 1. The steady state experiments were tested at constant temperature and different pressures. The heating experiments were operated at constant pressure, and the temperature is heating from about 23 °C to high temperature with a constant heat flux. The boost experiments were operated at constant temperature when the pressure increased from 6.5 to 11 MPa with an interval of 0.5 MPa. The depressurization experiments were operated at constant temperature when the pressure decreased from 11 to 6.5 MPa with an interval of 0.5 MPa.

2.2. Analytical methods and calculations

In this study, the intensity of light source is measured with a vacuum CO_2 container to eliminate the impact of the air. The non-transmissive ratio of the specific band of CO_2 is calculated by the transmitted light intensity across the CO_2 container with and without the light source. The non-transmissive ratio of the CO_2 is calculated by Eq. (1).

$$\varepsilon = 1\text{-}\frac{I_B - I_T}{I_s} \tag{1}$$

Here ε is the non-transmissive ratio of CO_2, I_B and I_T are the transmission intensity of the band across the CO_2 container with and without the light source, respectively, and I_s is the light source intensity measured with a vacuum CO_2 container.

The interference of ambient light and sapphire glass windows are removed by the vacuum light source test group. The non-transmissive ratio can be divided into the absorption ratio (σ) and the scattering ratio (δ). When the fluid field reaches a stable and uniform state at the steady state, the scattering ratio (δ) is equal to 0, and the absorption ratio is equal to the non-transmissive ratio [11]. Here, the scattering ratio (δ) is calculated by Eq. (2).

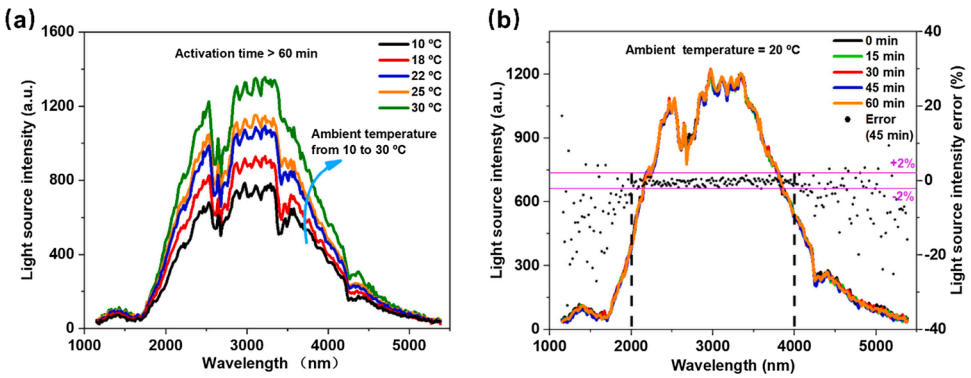

Fig. 3. Experiments with vacuum CO_2 container: (a) light source intensity with the activation time > 60 min at different ambient temperatures, (b) light source intensity with the activation time ranging from 0 min to 60 min at 20 °C and light source intensity measurement deviations for 45 min group.

$$\varepsilon = \sigma + \delta \tag{2}$$

The absorption ratio of CO_2 is impacted by the geometry of the container, the fluid properties, and the ambient factors. The impact of the ambient factors is eliminated by the light source intensity measured in the vacuum condition. Therefore, the absorption ratio σ can be calculated by the Lambert-Beer law as shown in Eq. (3).

$$\sigma = K \cdot C \cdot L \tag{3}$$

Here K is the molar absorption coefficient that depends on the wavelength, C is the fluid concentration, and L is the absorption thickness. The absorption ratio is mainly affected by the fluid concentration as the absorption thickness and molar absorption coefficient for a specific band are constant.

2.3. Stability validation of the light source and spectrometer

According to Eq. (1), the light source intensity and the spectrometer stability have significant impacts on the absorption ratio of characteristic CO_2 spectrum. However, the light source intensity changes significantly at different ambient temperatures, as shown in Fig. 3(a). To stabilize the light intensity, the ambient temperature of all experiments is controlled at 20 °C in this study. To validate the power stability of light source, the light intensity was measured with an activation time ranging from 0 to 60 min at a controlled ambient temperature of 20 °C. The measurement deviation of light source intensity is calculated by Eq. (4).

$$x_i = (1 - \frac{I_i}{I_b}) \times 100\% \tag{4}$$

Here x_i is the measurement deviation, I_i is the measured light source intensity for group i and I_b is the balance light source intensity measured with more than 60 min activation time. As shown in Fig. 3(b), the measurement deviations of light source intensity are within 2% for the wavelengths between 2000 and 4000 nm, which could be further reduced using a high precision spectrometer. According to the measurement deviation propagation law, the maximum calculation deviations of the non-transmissive ratio (x_ε), the absorption ratio (x_σ) and scattering ratio (x_δ) are calculated by Eqs. (5) and (6).

$$x_\sigma = x_\varepsilon = \sqrt{(x_B + x_T)^2 + (x_s)^2} \tag{5}$$

$$x_\delta = x_\sigma + x_\varepsilon \tag{6}$$

Here x_B, x_T and x_s are the measurement deviations of the transmissive intensities of parameters from Eq. (1). The maximum measurement deviations of the non-transmissive ratio, the absorption ratio and scattering ratio are ±4.48 %, ±4.48 % and ±8.96 %, respectively.

3. Results and discussion

3.1. Sensitivity analysis and measurement bands selection of infrared absorption spectrum at steady states

As a basic case, the steady state experiments were first conducted with the operating temperature and pressure changing from 25 to 55 °C and from 7.0 to 10.0 MPa, respectively. As shown in Fig. 4(a), the absorption ratio of CO_2 increased with the rise of operating pressure, while different infrared bands presented different variation characteristics. The bands of 2700–2800 nm at different pressures (7.0–10.0 MPa) presented high absorption ratios (> 0.8) at 45 °C, while the largest difference among them was smaller than 0.05. The bands of 3000–3100

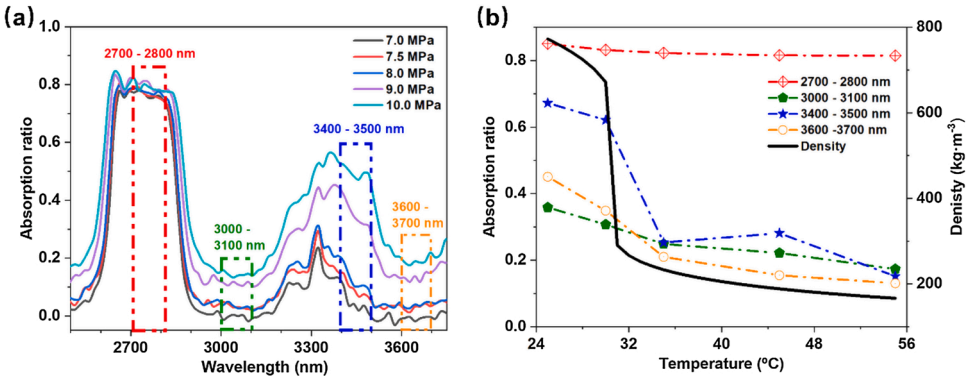

Fig. 4. The absorption ratio of the infrared spectrum between 2500 nm and 3700 nm: (a) working temperature at 45 °C, and pressures between 7.0 MPa and 10.0 MPa, (b) working pressure at 7.0 MPa, working temperatures between 25 and 55 °C.

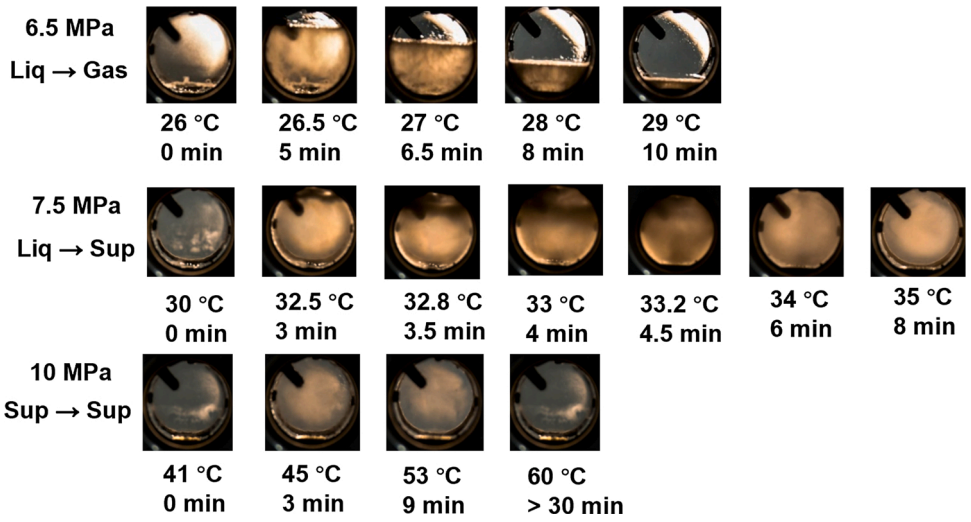

Fig. 5. The phenomenon of the flow fields with the rise of temperature at 6.5 MPa, 7.5 MPa and 10.0 MPa.

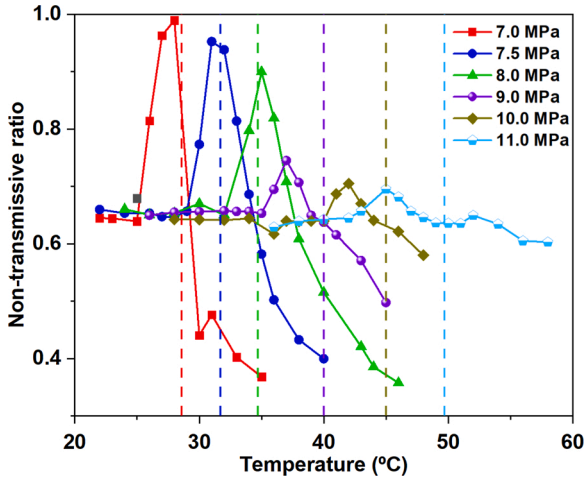

Fig. 6. The non-transmissive ratio of CO_2 at pressure ranging from 7.0 MPa to 11.0 MPa, and temperature between 20 and 60 °C within the wavelength of 3400 – 3500 nm, where the dash lines are the phase change or pseudo-critical temperatures.

nm and 3600–3700 nm presented low absorption ratios (< 0.1) at 45 °C and 7.0 MPa, whose differences between 7.0 and 10.0 MPa were both about 0.2. The bands of 3400–3500 nm presented the largest difference of the absorption ratio (~ 0.5) between 7.0 MPa and 10.0 MPa, which was two times larger than the bands of 3000−3100 nm. The absorption ratios of CO_2 in different infrared bands with the change of temperature were further presented in Fig. 4(b). The bands of 2700–2800 nm at 7 MPa presented low differences (< 0.05) of the absorption ratio between 25 and 55 °C. The maximum differences of the absorption ratio at bands of 3000−3100 nm, 3400–3500 nm and 3600−3700 nm at 7 MPa were 0.15, 0.30 and 0.55 between 25 and 55 °C, respectively. Besides, the density of CO_2 decreased from 800 to 170 kg m^{-3} when the temperature increased from 25 to 55 °C, where dramatic reductions of the density (- 70 %) and the absorption ratio (- 60 %) of the 3400–3500 nm bands were observed between 30 and 34 °C [12]. It is found that the absorption ratio could feed back the density changes more accurately than the temperature. Therefore, the bands of 3400–3500 nm were selected to analyze the experiment results in the dynamic experiments due to its sensitive response to the change of fluid density.

3.2. Dynamic characteristics of infrared absorption spectrum during the heating process

Scattering is caused by the messy refraction of light inside the fluid, which can be observed during the dramatic density change at pseudo-critical points. Photos of the flow fields at 6.5, 7.5 and 10.0 MPa were recorded as shown in Fig. 5. At 6.5 MPa, an obvious phase interface occurred at 26.5 °C and bubbles were generated at the bottom of the container, leading to the aggravation of scattering and contributed to the high non-transmission ratio (> 0.95) of CO_2. With the increase of temperature, the liquid level dropped quickly, and the scattering phenomenon was disappeared in the gaseous phase. At 7.5 MPa, density stratification was observed at 32.5 °C, which moved towards the bottom with the increase of temperature (33 °C). After the disappearance of density stratification, the fluid presented a strong density unevenness with an obvious scattering phenomenon. At 10.0 MPa, no density stratification was observed and there was only a slight scattering in the supercritical region, indicating a small density change.

To further explore the scattering characteristics near the pseudo-critical critical points, experiments were conducted at different pressures (6.5, 7.0, 7.5, 8.0, 9.0, 10.0 and 11.0 MPa) and the spectrum characteristics of the bands of 3400–3500 nm were measured at different temperatures (20–60 °C). As shown in Fig. 6, the peaks of CO_2 non-transmission ratios were observed near the pseudo-critical temperatures at different working pressures. However, the absorption ratio of CO_2 decreased with the rise of temperature as in accordance with Fig. 4(b). Therefore, the scattering appeared, reached a peak value with the temperature approaching the pseudo-critical point and disappeared with the further rise of temperature. The maximum non-transmission ratios were observed near the pseudo-critical points in 7.0, 7.5 and 8.0 MPa cases, while in 9.0, 10.0 and 11.0 cases, the maximum ratios were significantly declined and occurred in advance of the pseudo-critical points.

3.3. Dynamic characteristics of infrared absorption spectrum during the boost process

Working pressure variation is unavoidable but should be controlled during the startup, the shutdown and the load variation processes in the sCO_2 Brayton cycle [28]. To illustrate the changes of the flow field during the boost process, photos of the sectional view were recorded with the pressure increasing from 7.0 to 9.0 MPa as shown in Fig. 7. When the pressure increased from 7.0 to 7.5 MPa (at 30 °C), the injected CO_2 quickly filled the container, and reached the balance state in one

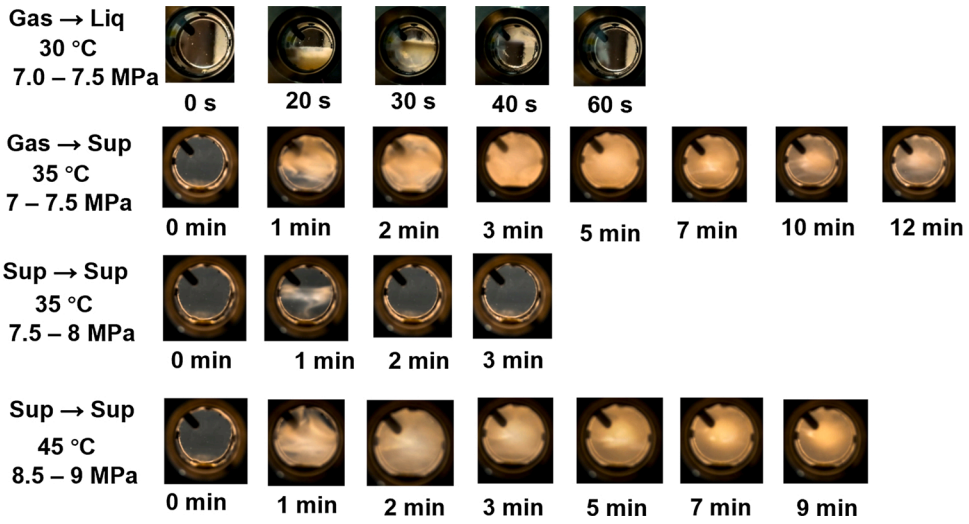

Fig. 7. The phenomena of the flow field with the rise of boost operation time at different conditions, including 7.0 -7.5 MPa (30 °C), 7.0 – 7.5 MPa (35 °C), 7.5 – 8.0 MPa (35 °C) and 8.5 – 9.0 MPa (45 °C).

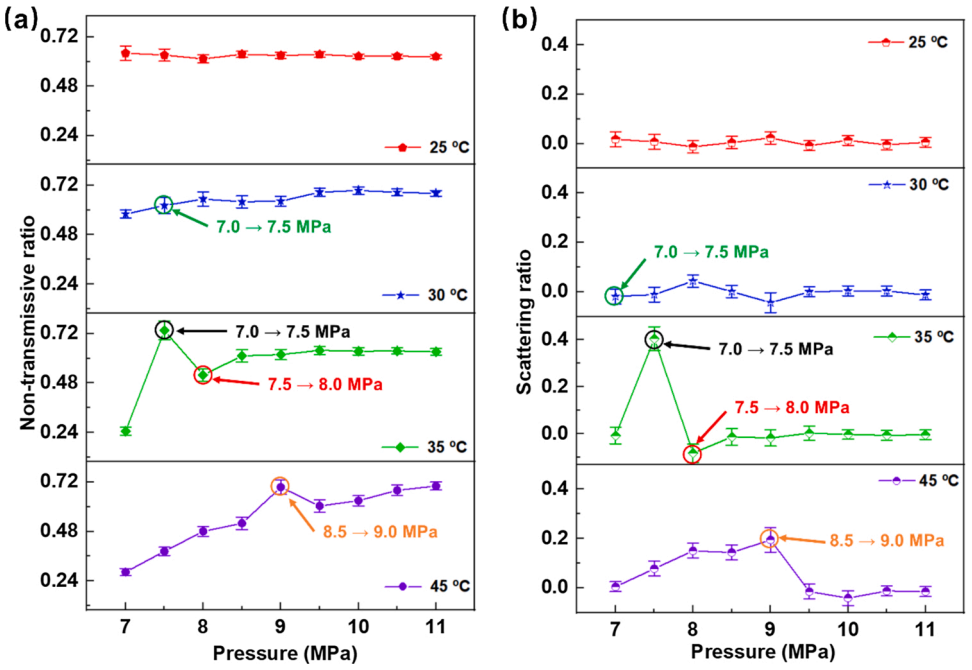

Fig. 8. Spectrum characteristics of CO_2 within the bands of 3400 - 3500 nm in one minute of boost operation with pressure ranging from 6.5 MPa to 11.0 MPa, and temperature between 25 and 45 °C: (a) non-transmissive ratio, (b) scattering ratio.

minute. When the pressure increased from 7.0 to 7.5 MPa, scattering phenomenon was observed with the injection of high-pressure CO_2, which mixed with the exited CO_2 and gradually reached a state balance after 12 min. When the pressure increased from 7.5 to 8.0 MPa, the injected CO_2 diffused quickly and reached a uniform state within two minutes. There was no significant scattering observed in this process due to the small density change. With the further pressure increase from 8.5 to 9.0 MPa, significant scattering near the pseudo-critical pressure occurred again, and a long time was needed before the mixed CO_2 could reach a uniform state.

To further study the scattering of CO_2 with the rise of working pressure, pressure boost experiments with fluid injection were performed at different pressures (6.5–11.0 MPa) and temperatures (25–45 °C). Fig. 8(a) presented the non-transmissive ratio variation tendency of CO_2 in the boosting experiments with the working pressure rising from 6.5 MPa to 11.0 MPa and the cases from Fig. 7 within the circles. The non-transmissive ratio (~0.65) was relative constant at 25 °C, while it continued to increase with the rise of pressure at 30 °C. At 35 °C and 45 °C, obvious non-transmissive peaks (~ 0.7) were observed near the pseudo-critical pressures. This can be explained by the decrease of the maximum CO_2 density difference between 6.5 and 11.0 MPa with the increase of temperature as has been presented in Fig. 1. The scattering ratios at different temperatures were further presented in Fig. 8(b), where the scattering occurred near the pseudo-critical temperature and then disappeared with the operating temperature moving away from the pseudo-critical temperature.

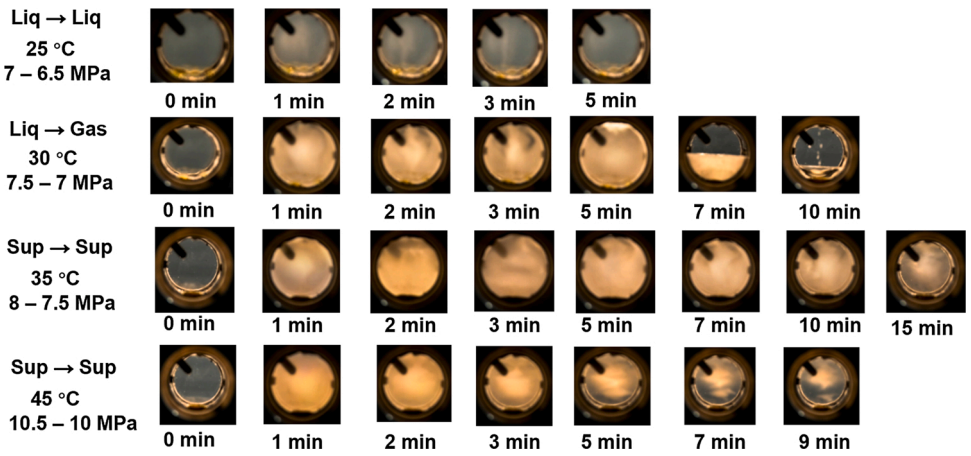

Fig. 9. The phenomenon of scattering varied with the rise of depressurization operation time at different conditions, including 7.0 – 6.5 MPa (25 °C), 7.5 – 7.0 MPa (30 °C), 8.0 – 7.5 MPa (35 °C) and 10.5 – 10.0 MPa (45 °C).

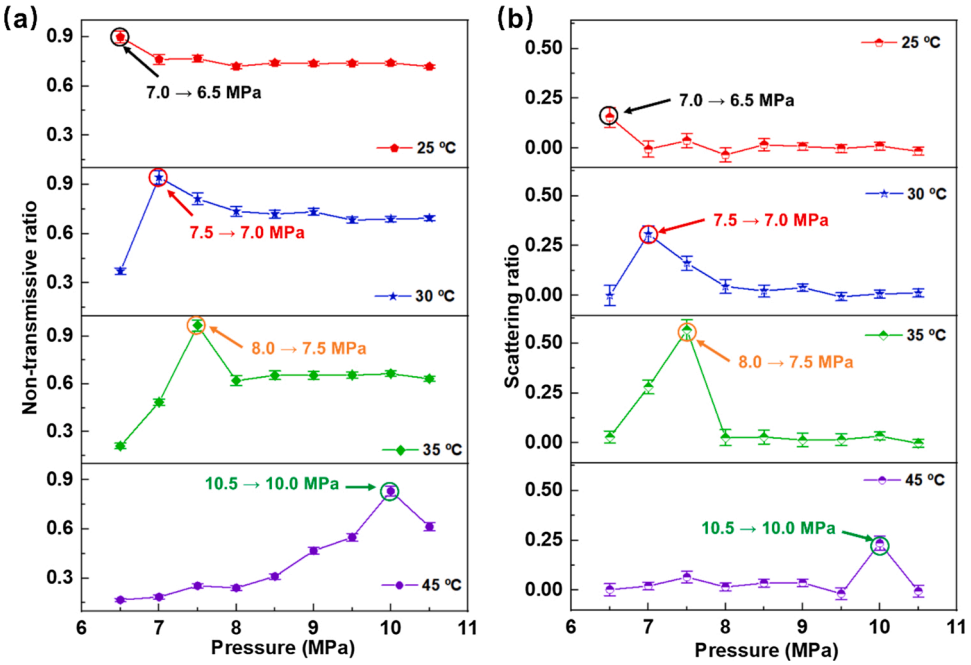

Fig. 10. Spectrum characteristics of CO_2 within the bands of 3400 - 3500 nm in one minute of depressurization operation with pressure ranging from 6.5 MPa to 11.0 MPa, and temperature between 25 and 45 °C: (a) The non-transmissive ratio and (b) scattering ratio.

3.4. Dynamic characteristics of infrared absorption spectrum during the depressurization process

Boost process is accompanied with the fluid injection, while depressurization process is accompanied with the fluid discharging. To learn the changes of the flow field during the depressurization process, photos of the sectional view were recorded with 0.5 MPa depressurization processes at different pressures and temperatures as shown in Fig. 9. When the pressure decreased from 7.0 to 6.5 MPa (at 25 °C), slight scattering was observed and disappeared in 5 min. When the pressure decreased from 7.5 to 7.0 MPa (at 30 °C), strong scattering was observed in one minute, and phase interface occurred in the 5th minutes with strong boiling in the liquid region and disappeared after 10 min. The gasification time was more than five times longer than the liquefaction time, which explained the stronger scattering observed in the depressurization processes. When the pressure decreased from 8.0 to 7.5 MPa (35 °C), fluid left the container and caused chaotic internal flow. The scattering gradually disappeared after 15 min, which was longer than the 45 °C group.

To further study the scattering of CO_2 in the depressurization operations, experiments were performed at pressures of 6.5–11.0 MPa and temperatures of 25–45 °C. As shown in Fig. 10(a), the non-transmissive ratios reached peaks near the phase changing or pseudo-critical points identified with circles in the depressurization experiments with the working pressure decreasing from 11.0 MPa to 6.5 MPa, which were the cases shown in Fig. 9. Different from the boost experiments, depressurization operation caused significant non-transmissive variation at 25 and 30 °C, where peaks were observed. At 35 °C, strong non-transmissive peaks (~0.95) were observed at 9.0 MPa, which was similar with the boost experiments. The non-transmissive peak (~0.85) appeared at 10.0 MPa (the pseudo-critical point) in the depressurization operation at 45 °C, while the peak of boost experiments was appeared in 9.0 MPa. Therefore, the scattering ratios at different temperatures were further presented in Fig. 10(b), where the scattering occurred near the pseudo-critical temperature and then disappeared with the operating temperature moving away from the pseudo-critical temperature.

Compared with boost experiments, stronger scattering was observed near the pseudo-critical pressure at different temperatures. Overall, scattering was unavoidable during the heating, the boost and the depressurization progresses near the pseudo-critical points, which strengthened the non-transmissive ratio of CO_2 during abnormal conditions and could give strong signals timely.

4. Conclusions

In this study, the absorption spectrum of CO_2 at steady state and the scattering of CO_2 during dynamic (heating, boost and depressurization) processes were studied using the infrared spectra measure method. The absorption spectrum near 3400 nm wavelength was found to give a clear feedback to the state change of the CO_2. The density of CO_2 decreased from 800 to 170 kg m^{-3} when the temperature increased from 25 to 55 °C, where dramatic reductions of the density (- 70 %) and the absorption ratio (- 60 %) of the 3400–3500 nm bands were observed between 30 and 34 °C. The absorption ratio could feed back the density changes more accurately than the temperature. Dramatic scattering phenomenon was observed near the pseudo-critical point in the heating, the boost and the depressurization processes. This phenomenon could serve as a warning signal during the abnormal conditions as the non-transmissive ratio of CO_2 was significantly increased in the liquid or supercritical region. Density stratification was only observed at 32.5 °C and 7.5 MPa in the heating process when the condition was close to the critical point. Besides, the liquefaction time was shorter than 1 min, which could be ignored in the boost process. And the gasification time was more than five times longer than the liquefaction time, which explained the stronger scattering observed in the depressurization processes. As a non-contact measurement method, the infrared spectra could detect the density change instantly without interfering fluid flows without interference the flow field. It could also improve the control accuracy of the operating parameters and provide sensitive warning function for abnormal conditions by monitoring the density changes.

Overall, the infrared spectra measure method seems potential for the application in sCO_2 Brayton cycle and many other scenarios to monitor the transient state of CO_2 near the critical point. More researches are needed to develop a practical method with a specified software and enough experimental data.

CRediT authorship contribution statement

Kaixiang Xing: Conceptualization, Methodology, Investigation, Resources, Data curation, Writing - original draft, Writing - review & editing. **Yuxuan Ji:** Investigation, Data curation. **Zheng Wang:** Investigation, Data curation. **Mingxuan Wang:** Investigation, Data curation. **Yafei Liu:** Investigation, Data curation. **Haoran Xu:** Writing - review & editing, Visualization. **Gang Xiao:** Methodology, Formal analysis, Writing - review & editing.

Declaration of Competing Interest

The authors declare that they have no known competing financial interests or personal relationships that could have appeared to influence the work reported in this paper.

Acknowledgements

The authors gratefully acknowledge the support from the National Natural Science Foundation of China (No. 51776186) and Zhejiang Provincial Natural Science Foundation (NO. LR20E060001).

References

[1] R. Penthala, G. Heo, H. Kim, I.Y. Lee, E.H. Ko, Y.-A. Son, Synthesis of azo and anthraquinone dyes and dyeing of nylon-6,6 in supercritical carbon dioxide, J. CO2 Util. 38 (2020) 49–58.
[2] M. Safder, F. Temelli, A. Ullah, Supercritical CO2 extraction and solvent-free rapid alternative bioepoxy production from spent hens, J. CO2 Util. 34 (2019) 335–342.
[3] I. Ishak, N. Hussain, R. Coorey, M.A. Ghani, Optimization and characterization of chia seed (Salvia hispanica L.) oil extraction using supercritical carbon dioxide, J. CO2 Util. 45 (2021), 101430.
[4] V. Zare, M. Hasanzadeh, Energy and exergy analysis of a closed Brayton cycle-based combined cycle for solar power tower plants, Energy Convers. Manage. 128 (2016) 227–237.
[5] W. Song, H. Ni, R. Wang, B. Sun, Z. Shen, Pressure transmission in the tubing of supercritical carbon dioxide fracturing, J. CO2 Util. 21 (2017) 467–472.
[6] N.T. Rao, A.N. Oumer, U.K. Jamaludin, State-of-the-art on flow and heat transfer characteristics of supercritical CO2 in various channels, J. Supercrit. Fluid. 116 (2016) 132–147.
[7] L. Teng, Y. Xuan, Design of a composite receiver for solar-driven supercritical CO2 Brayton cycle, J. CO2 Util. 32 (2019) 290–298.
[8] H.R. Abbasi, A. Yavarinasab, S. Roohbakhsh, Waste heat management of direct carbon fuel cell with advanced supercritical carbon dioxide power cycle – a thermodynamic-electrochemical modeling approach, J. CO2 Util. 51 (2021), 101630.
[9] Y. Ahn, S.J. Bae, M. Kim, S.K. Cho, S. Baik, J.I. Lee, et al., Review of supercritical CO_2 power cycle technology and current status of research and development, Nucl. Eng. Technol. 47 (2015) 647–661.
[10] M. Mecheri, Y. Le Moullec, Supercritical CO_2 Brayton cycles for coal-fired power plants, Energy 103 (2016) 758–771.
[11] S. Wang, J. Si, Z. Hu, G. Li, Z. Zhang, B. Fang, J. Ye, J. Shao, Multi-beam interferometric Rayleigh scattering technique for simultaneous 2-D quantitative measurement of multi-parameters in high speed flow field, Opt. Commun. 495 (2021), 127069.
[12] E.W. Lemmon, M.L. Huber, M.O. McLinden, NIST Standard Reference Database 23: Reference Fluid Thermodynamic and Transport Properties-REFPROP, Version 9.1, National Institute of Standards and Technology, Gaithersburg, 2013.
[13] E.M. Clementoni, T.L. Cox, Practical aspects of supercritical carbon dioxide Brayton system testing, in: The 4th International Symposium – Supercritical CO_2 Power Cycles, Pittsburgh, Pennsylvania, 2014.
[14] A. Einstein, Eine neue Bestimmung der Moleküldimensionen, Ann. Phys. 324 (1906) 18.
[15] S.A. Egorov, Local density enhancement in neat supercritical fluids: dependence on the interaction potential, Chem. Phys. Lett. 354 (2002) 140–147.
[16] M. Musso, F. Matthai, D. Keutel, K.-L. Oehme, Critical Raman line shape behavior of fluid nitrogen, Pure Appl. Chem. 76 (2004) 147–155.
[17] T. Kunihiro, Y. Minami, K. Tsumura, Critical opalescence around the QCD critical point and second-order relativistic hydrodynamic equations compatible with boltzmann equation, Nucl. Phys. A 830 (2009) 207c–210c.
[18] B.A. Salinas, H.A. Sathish, S.M. Bishop, N. Harn, J.F. Carpenter, T.W. Randolph, Understanding and modulating opalescence and viscosity in a monoclonal antibody formulation, J. Pharm. Sci. 99 (2010) 82–93.
[19] M.Y. Sushko, Critical opalescence in fluids: 1.5-Scattering effects and the Landau–Placzek ratio, J. Mol. Liq. 163 (2011) 33–35.
[20] H. Nakayama, K.-i Saitow, M. Sakashita, K. Ishii, K. Nishikawa, Raman spectral changes of neat CO2 across the ridge of density fluctuation in supercritical region, Chem. Phys. Lett. 320 (2000) 323–327.
[21] V.G. Arakcheev, V.B. Morozov, Narrowing of the vibrational spectrum under compression of liquid carbon dioxide, JETP Lett. 90 (2009) 524–529.
[22] V.G. Arakcheev, V.N. Bagratashvili, A.A. Valeev, V.B. Morozov, V.K. Popov, Broadening peculiarities of vibrational bands in the spectrum of carbon dioxide close to the critical temperature, Russ. J. Phys. Chem. B 4 (2011) 1245–1251.
[23] Y.A. Chaikina, Broadening of vibration Q-bands in the Raman spectrum of carbon dioxide due to critical density fluctuations, Russ. J. Phys. Chem. B 10 (2017) 1039–1047.
[24] Y.A. Chaikina, Molecular model for critical opalescence of carbon dioxide, Russ. J. Phys. Chem. B 12 (2019) 1182–1192.
[25] J.A. Chaikina, S.Y. Umanskii, Peculiarities of the small-angle scattering of laser radiation by critical CO2, Chem. Phys. 536 (2020), 110795.
[26] X. Yu, Z. Dong, J.K.W. Yang, Q.J. Wang, Room-temperature mid-infrared photodetector in all-carbon graphene nanoribbon-C60 hybrid nanostructure, Optica 3 (2016) 979–984.
[27] A.D. Román-Ospino, R. Singh, M. Ierapetritou, et al., Near infrared spectroscopic calibration models for real time monitoring of powder density, Int. J. Pharm. 512 (2016) 61–74.
[28] G. Fan, H. Li, Y. Du, K. Chen, S. Zheng, Y. Dai, Preliminary design and part-load performance analysis of a recompression supercritical carbon dioxide cycle combined with a transcritical carbon dioxide cycle, Energy Convers. Manage. 212 (2020), 112758.